Nanoscale

View Online
Dynamic Article Links

Cite this: *Nanoscale*, 2011, **3**, 3159

www.rsc.org/nanoscale

PAPER

Annealing effects on the photovoltaic performance of all-conjugated poly(3-alkylthiophene) diblock copolymer-based bulk heterojunction solar cells†

Ming He,[ab] Wei Han,[ac] Jing Ge,[b] Weijie Yu,[a] Yuliang Yang,[b] Feng Qiu[b] and Zhiqun Lin*[ac]

Received 18th March 2011, Accepted 3rd May 2011
DOI: 10.1039/c1nr10293a

The effects of thermal and solvent vapor annealing on the photovoltaic performance of a new class of all-conjugated poly(3-butylthiophene)-*b*-poly(3-hexylthiophene) diblock copolymer/$PC_{71}BM$ bulk heterojunction (BHJ) solar cells were scrutinized and theoretically analyzed using the single diode model combined with experimental measurements. The meanings of physical parameters in the model were elucidated in the context of crystalline order and phase separation to gain fundamental insight into the mechanism of annealing effects on the device performance of a new class of all-conjugated diblock copolymer-based BHJ solar cells.

Introduction

The performance of polymer bulk heterojunction (BHJ) solar cells has been significantly improved over the past decade. Recently, considerable efforts have centered on understanding the photovoltaic mechanism that underpins these enhanced power conversion efficiencies (*PCEs*).[1–6] One of the most widely studied polymer BHJ solar cells utilizes poly(3-hexylthiophene) (P3HT) as the electron donor and fullerene derivative (*i.e.*, [6,6]-phenyl-C_{61}-butyric acid ethyl ester (PCBM)) as the electron acceptor. Reproducible, high efficiency ($PCE = 3\sim5\%$) can be readily achieved by performing various post treatments on these devices, including the application of thermal annealing[7,8] and solvent vapor annealing,[9,10] the use of solvent additives,[11] *etc.* It has been widely recognized that annealing, including both thermal and solvent vapor annealing, are of critical importance in optimizing the film morphology of the P3HT/PCBM blend by facilitating the nanoscale phase separation of P3HT and PCBM (*i.e.*, producing small-sized domains that are comparable to or less than the exciton diffusion length of conjugated polymers (~10 nm) and a large interface between P3HT and PCBM) for efficient exciton dissociation and charge generation, and yielding the molecular packing of P3HT chains within the photoactive layer to form percolation networks for efficient charge transport and collection without significant recombination loss.[3,12]

It is noteworthy that the solubility of poly(3-alkylthiophene) (P3AT) homopolymers is dictated by the length of alkyl side chains, which exerts a profound influence on the phase separation and interfacial interaction between P3ATs and PCBM during the annealing process.[13] Recently, better optimized polymer BHJ nanostructures in a new class of all-conjugated poly(3-butylthiophene)-*b*-poly(3-hexylthiophene) diblock copolymer (P3BHT)-based devices were reported,[14] where the solubility can be readily tuned by adjusting the molar ratio of P3BT to P3HT blocks, leading to markedly improved photovoltaic performance of P3BHT/[6,6]-phenyl-C_{71}-butyric acid ethyl ester ($PC_{71}BM$) solar cells. A comprehensive study on the effect of changes in the ratio of butyl to hexyl side chains in P3BHT on the blend film morphology and the resulting device performance was performed. The study revealed that the P3BHT diblock copolymer at the P3BT: P3HT = 2 : 1 molar ratio, denoted P3BHT21, which exhibited an improved performance over the P3HT/$PC_{71}BM$ solar cell prepared under the same conditions, was able to accomplish a better balance between the chain flexibility that rendered effective exciton dissociation and charge generation (*i.e.* forming fine phase separation on the 10-nm scale) and the crystallization of P3BHT21 chains that facilitated efficient charge transport and collection.[14,15]

Herein, using the single diode model,[4] we scrutinized and theoretically analyzed the effects of thermal annealing and solvent vapor annealing on the photovoltaic performance of all-conjugated P3BHT21 diblock copolymers blended with $PC_{71}BM$. The meanings of physical parameters yielded from the fitting of the electrically equivalent single diode model were elucidated in the context of phase separation and crystallization to gain fundamental insight into the possible photophysical

[a]*Department of Materials Science and Engineering, Iowa State Univerisity, Ames, IA, 50010. E-mail: zqlin@iastate.edu*
[b]*The Key Laboratory of Molecular Engineering of Polymers, Ministry of Education, Department of Macromolecular Science, Fudan Univeristy, Shanghai, 200433, China*
[c]*School of Materials Science and Engineering, Georgia Institute of Technology, Atlanta, GA, 30332. E-mail: zhiqun.lin@mse.gatech.edu*
† Electronic supplementary information (ESI) available: Experimental details on device fabrication and evaluation. See DOI: 10.1039/c1nr10293a

mechanisms responsible for the varied performances, which were further verified experimentally by the X-ray diffraction, UV-Vis absorption and AFM measurements.

Experimental

Photovoltaic devices with the configuration of ITO/poly(3,4-ethylenedioxythiophene): poly(styrenesulfonate) (PEDOT:PSS)/P3BHT21:$PC_{71}BM$/Ca/Al were fabricated at the P3BHT:$PC_{71}BM$ =1 : 0.75 wt/wt (Fig. 1 and See *Experimental* in Supporting Information). The thickness of PEDOT:PSS, P3BHT21:$PC_{71}BM$, Ca, and Al layers are approximately 40 nm, 200 nm, 50 nm, and 100 nm, respectively. Typically, the device area was 0.10 ± 0.01 cm^2. In the present study, a series of devices without annealing treatment (*i.e.*, pristine sample), with thermal annealing at 140 °C for 20 min, and with $CHCl_3$ vapor annealing for 12 h, respectively, were evaluated under a simulated AM 1.5 G irradiation (100 mW cm^{-2}, calibrated with Daystar Meter).

Fig. 2 shows the current density-voltage (*J–V*) characteristics of devices. The photovoltaic performances were summarized in Table 1. A remarkable increase in J_{sc} and *FF* emerged upon thermal annealing (red circles), compared with the pristine device without annealing (black squares). The maximum *PCE* of 3.81% was obtained in the thermally annealed device with V_{oc} of 0.65 V, J_{sc} of 9.56 mA cm^{-2} and *FF* of 61.7%. The higher *FF* suggested that thermal annealing promoted the blend film to achieve improved BHJ nanostructures with well-defined demixing of two components and extended percolation networks for each component.[16,17] Quite intriguingly, compared the performance of solvent vapor annealed device (blue triangles) with pristine (black squares) and thermally annealed devices (red circles), a strong increase of J_{sc} from 8.29 mA cm^{-2} to 10.9 mA cm^{-2} with a decrease of V_{oc} from 0.63 V to 0.53 V after annealed with $CHCl_3$ vapor for 12 h was observed. The highest J_{sc} obtained after solvent vapor annealing could be primarily related to an increased crystallinity of P3BHT21 in the blend film (Fig. 3a). The XRD profiles of P3BHT21 in the blend films before and after thermal annealing exhibited a distinct single [100] peak at

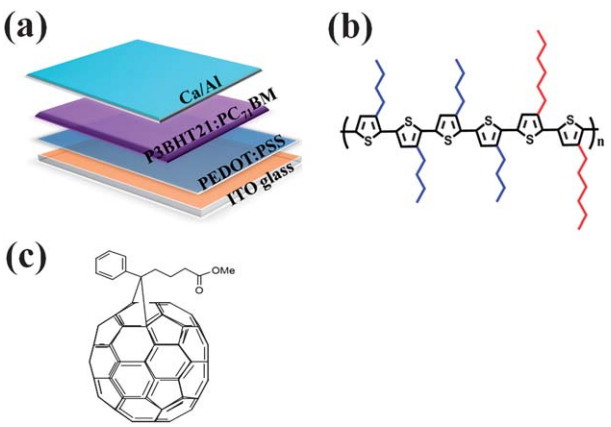

Fig. 1 (a) The configuration of P3BHT21/$PC_{71}BM$ BHJ solar cells, in which the weight ratio of P3BHT21 to $PC_{71}BM$ is 1 : 0.75. (b) The chemical structure of poly(3-butylthiophene)-*b*-poly(3-hexylthiophene) (P3BHT21) diblock copolymer with a molar ratio of P3BT block to P3HT block = 2 : 1. (c) The chemical structure of $PC_{71}BM$.

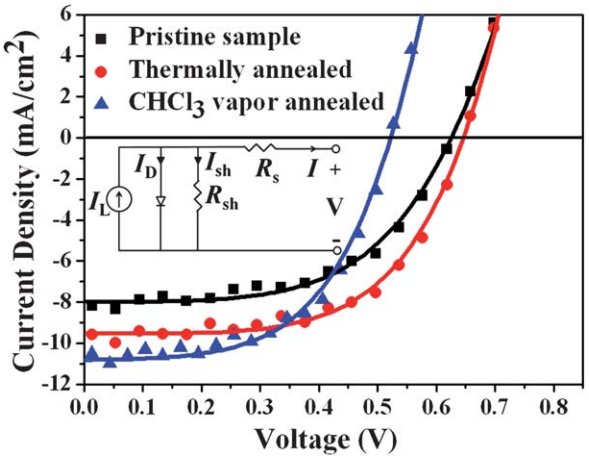

Fig. 2 Current density-voltage (*J–V*) characteristics of P3BHT21/$PC_{71}BM$ solar cells without annealing treatment (squares), with thermal annealing at 140 °C for 20 min (cycles), and with chloroform vapor annealing for 12 h (triangles). The solid curves are the corresponding theoretical fits to the experimental data in symbols. The single diode model is depicted in the inset.

Table 1 Summary of photovoltaic performances of P3BHT21/$PC_{71}BM$ solar cells without annealing treatment, with thermal annealing at 140 °C for 20 min, and with chloroform vapor annealing for 12 h, respectively

P3BHT21/$PC_{71}BM$	V_{oc} (V)	J_{sc} (mA cm^{-2})	FF (%)	PCE (%)
Pristine sample	0.63	8.29	54.4	2.83
Thermally annealed	0.65	9.56	61.7	3.81
$CHCl_3$ vapor annealed	0.53	10.9	58.9	3.25

$2\theta = 6.5°$, corresponding to the d-spacing of 13.2 Å, which indicated that the P3BT and P3HT blocks co-crystallized into a lamellar packing with the interdigitation of butyl and hexyl side chains one another,[18] adopting the edge-on orientation with the thienyl backbone aligned parallel to the substrate (inset in Fig. 3a).[19] A slight peak shift from $2\theta = 6.5°$ to 6.3° was observed in the blend film after $CHCl_3$ vapor annealing, corresponding to a slightly increased d-spacing of 13.8 Å. This demonstrated that the molecular packing of P3BHT21 was not significantly affected by the thermal annealing, but the inter-chain distance of alkyl side chains along [100] axis could be enlarged by the solvent vapor annealing. Considering the thicknesses of all blend films were approximately 200 nm, the intensity of the [100] peak in Fig. 3a was nearly proportional to the size or the number of polymer crystals per unit volume in the blend films,[20] and the highest crystallinity of P3BHT21 in the blend film with $CHCl_3$ vapor treatment was responsible to the largest J_{sc} observed in the vapor-annealed devices (Table 1).[21] Despite the increased J_{sc}, however, a decreased V_{oc} with the $CHCl_3$ vapor treatment was seen and needed to be addressed.

To explore the origin of the reduced V_{oc}, the *J–V* characteristics of devices (Table 1) were fitted with the electrically equivalent single diode model (inset in Fig. 2), which consists of a diode (with reverse saturation current, I_D, and ideality factor, *n*) and photogenerated current, I_L, representing an ideal photovoltaic device. Considering no device can actually reach the ideal

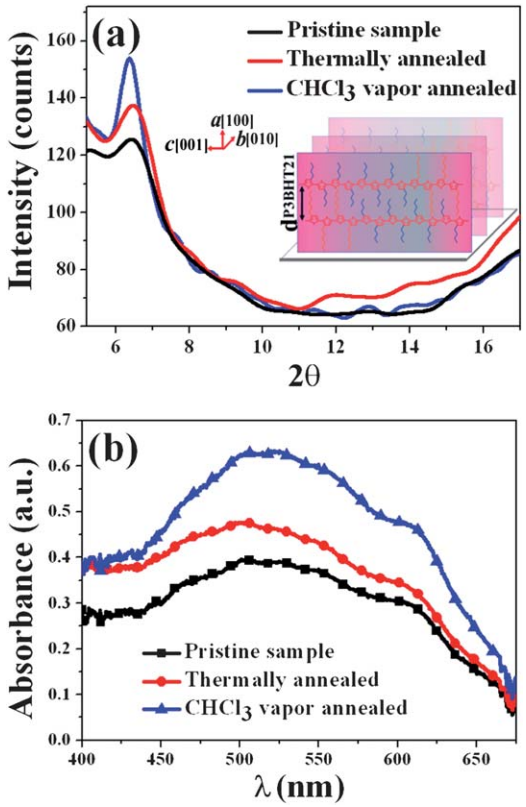

Fig. 3 (a) XRD profiles of P3BHT21/$PC_{71}BM$ blend films without annealing treatment (*i.e.*, pristine sample), with thermal annealing at 140 °C for 20 min, and with chloroform vapor annealing for 12 h, respectively. The inset shows the molecular packing of P3BHT21 chains with the edge-on orientation. And (b) the corresponding UV-Vis spectra of P3BHT21 in the related blend films.

state, a shunt resistance, R_{sh} and a series resistance, R_s are introduced in the model.[4] The values of I_L, I_D, R_{sh}, and R_s are dependent on the area of device. In order to compare devices of different size and have the derived parameters in a similar order of magnitude with those of J–V curves, the characteristic equation of the single diode model is written in the form of the current density and the voltage.[22,23]

$$J = J_L - J_D\left\{\exp\left[\frac{q(V + Jr_s)}{nkT}\right] - 1\right\} - \frac{V + jr_s}{r_{sh}} \qquad (1)$$

where J is the current density, V is the applied voltage, J_L is the photogenerated current density, J_D is the reverse saturation current density, r_s is the specific series resistance, r_{sh} is the specific shunt resistance, n is the diode ideality factor, q is the elementary charge, k is the Boltzmann's constant, and T is the absolute temperature. The parameters of J_L, J_D, n, r_s and r_{sh} can be extracted from the nonlinear least-square fits to the photovoltaic J–V curves. The fitting agreed very well with the experimental results (Fig. 2). The fitting parameters are summarized in Table 2. In polymer BHJ solar cell, the current density, J is dictated by the portion of photogenerated charge carriers that can reach the appropriate electrodes within their lifetimes.[24] Based on the single diode model, the photogenerated current density, J_L qualitatively reflects the efficiency of exciton diffusion and charge generation in the device.[24] As the thicknesses of all devices were the same (200 nm) in the study, the highest J_L of 11.2 mA cm^{-2} in the solvent vapor annealed device suggested that the crystallinity of P3BHT21 in the blend film was significantly increased after exposure to the $CHCl_3$ vapor, even higher than that of its thermally annealed counterpart, which was consistent with the XRD results. It has been demonstrated that the improved crystallinity enhanced the absorption in the longer wavelength region near the band edge of polymers more significantly than that of thermal annealing;[3,25] this was verified by performing UV-Vis absorption measurements as shown in Fig. 3b. The highest absorption intensity of P3BHT21 in the solvent vapor annealed device signified that more ordered molecular packing of P3BHT chains were obtained with the $CHCl_3$ vapor, leading to increased J_L in the blend film.

We now turn our attention to address the change in V_{oc} of devices. As the shunt resistance is rather high, V_{oc} is mainly determined by the property of diode.[22]

$$V_{OC} = \frac{nkT}{q}\ln\left(\frac{J_{SC}}{J_D} + 1\right) \qquad (2)$$

Based on the traditional diode theory, the ideality factor n describes how closely the behavior of a diode matches an ideal diode where no recombination occurs ($n = 1$). In polymer BHJ solar cells, n is suggested to be characteristic of the recombination behavior in the blend film, and, correspondingly, a change in n serves as a measure of the presence of different type of mechanism for the recombination loss.[26–28] The n values do not vary much in different devices (Table 2), indicating that all blend films possessed BHJ nanostructures with a similar recombination mode. Clearly, both thermal and solvent vapor annealing did not alter the nanoscale demixing in the photoactive layer, which would otherwise exhibit an n value near 10 as in a microphase separated blend film.[14] The reverse saturation current density, J_D is of a measure of the carrier leakage in the vicinity of the barrier caused by recombination, occurring at the donor/acceptor interface.[28] It can be easily calculated that the variation of J_{SC}/J_D by a factor of 2 after solvent vapor annealing is equivalent to a change of V_{oc} from 0.63 V to 0.53 V (Table 1 and 2).[27] The reduction in V_{oc} may be rationalized as follows. Upon $CHCl_3$ vapor annealing, the crystallinity of P3BHT21 largely increased, and the interpenetrating networks available for respective

Table 2 Summary of photovoltaic parameters of the single diode model extracted from the J–V characteristics of P3BHT21/$PC_{71}BM$ solar cells without annealing treatment, with thermal annealing at 140 °C for 20 min, and with chloroform vapor annealing for 12 h, respectively

P3BHT21/$PC_{71}BM$	J_L (mA cm^{-2})	J_D (mA cm^{-2})	n	r_s (Ω cm^2)	r_{sh} (Ω cm^2)	PCE (%)
Pristine sample	8.47	0.032	4.32	3.10	1.38×10^3	2.83
Thermally annealed	9.91	0.021	4.06	1.49	1.41×10^3	3.81
$CHCl_3$ vapor annealed	11.2	0.049	3.74	1.83	0.64×10^3	3.25

electron and hole transports became unbalanced.[3] Therefore a higher degree of charge recombination occurred in the blend film (*i.e.*, increased interfacial charge leakage), representing a large J_D, and thus decreased V_{oc}.

To confirm the analysis as noted above, AFM measurements on the blend films were performed by examining the film morphology and structural order in the BHJ solar cells before and after annealing (Fig. 4). It is clearly evident that all blend films revealed nanoscale phase separation composed of grain-like P3BHT21 crystalline domains. Compared to the pristine sample (inset in Fig. 4a), the crystalline P3BHT21 domains were denser and the domain size became smaller after thermal annealing (*i.e.*, a finer scale of phase separation; inset in Fig. 4b), which can be attributed to the higher ordered molecular packing of P3BHT21 chains.[29] Quantitatively, the average size of P3BHT21 crystalline domains decreased from 12.8 nm without annealing to 10.9 nm with thermal annealing in the blend film, calculated from the full width at half-maximum (FWHM) of the diffraction peaks in Fig. 3a. Moreover, much more crystalline domains emerged in the $CHCl_3$ vapor annealed blend film (inset in Fig. 4c), correlating very well with the increased XRD peak (Fig. 3a) and enhanced optical absorption observed (Fig. 3b). We note that no dewetting or defects were observed in the blend film after solvent annealing (Fig. 4c and Figure S1 in Support Information). However, the crystalline domain size of P3BHT21 in the vapor-treated film appeared to grow larger (inset in Fig. 4c), from 12.8 nm without annealing to 18.8 nm with vapor annealing in the blend based on the FWHM calculations, which may result in poor phase separation (*i.e.*, a large-scale demixing) and increased charge recombination (*i.e.*, increased J_D; Table 2). As a result, it can be concluded that $CHCl_3$ vapor greatly promotes the crystallization of P3BHT21 chains, leading to increased optical absorption (blue curve in Fig. 3b) with improved J_L, and, conversely, the increased P3BHT21 crystalline domain size would suppress the diffusion of $PC_{71}BM$ molecules in the blend film to form nanoscale phase separation with P3BHT21 crystalline domains,[30] limit the formation of the $PC_{71}BM$ network,[28] and perturb the balance of electron and hole transport (*i.e.*, faster hole transport through the P3BHT21 phase due to the large-size crystalline P3BHT as compared to slower electron transport through the $PC_{71}BM$ phase due to constrained formation of percolation network), thereby resulting in increased reverse saturation current, J_D, and thus reduced V_{oc}. The surface roughness of active layer (*i.e.*, the active layer/cathode interface) may also be affected by different annealing treatments, resulting in a crucial influence on the *PCE*. The AFM height images of the P3BHT21/$PC_{71}BM$ blend films before and after annealing treatments are shown in Figure S1 (See Supporting Information). It is clear that thermal annealing slightly smoothed the surface of P3BHT21/$PC_{71}BM$ blend film, while solvent annealing made the surface rougher. The rougher surface after solvent annealing may originate from the formation of enhanced ordering of polymer structures (*i.e.*, enhanced crystallinity of P3BHT21).[31]

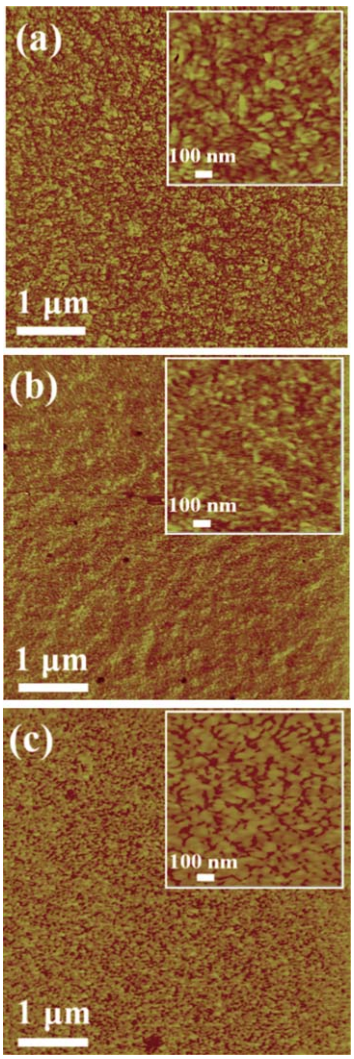

Fig. 4 Tapping mode AFM phase images of the P3BHT21/$PC_{71}BM$ blend films. (a) without annealing treatment, (b) with thermal annealing at 140 °C for 20 min, and (c) with chloroform vapor annealing for 12 h. The scanning size = 5 × 5 μm² for all images, and 1 × 1 μm² for all insets.

Conclusions

In conclusion, the effects of thermal annealing and solvent vapor annealing on the performance of P3BHT21/$PC_{71}BM$ BHJ solar cells were theoretically analyzed by the single diode model and experimentally explored by X-ray diffraction, UV-Vis absorption and AFM studies. Thermal annealing achieved a better balance between increased ordered packing of P3BHT21 chains and finer nanoscale phase separation in the P3BHT21/$PC_{71}BM$ blend film. In the case of $CHCl_3$ vapor annealing, although the treatment further improved the crystallization of P3BHT21 chains as compared to thermal annealing, larger crystalline P3BHT21 domains suppressed the dispersion of $PC_{71}BM$ molecules in the blend film, resulting in unbalanced respective electron and hole transports and thus increased charge recombination. The present integrated study *via* experimental measurements and theoretical modeling may provide much physical insight into the mechanism responsible for charge generation and transport in the polymer BHJ solar cells. The single diode model demonstrated in this work can be implemented to guide the optimization of processing parameters for fabrication of high-efficiency photovoltaic devices.

Acknowledgements

We gratefully acknowledge support from the National Science Foundation (NSF-CBET 0824361).

Notes and references

1 J. Xu, J. Wang, M. Mitchell, P. Mukherjee, M. Jeffries-El, J. W. Petrich and Z. Q. Lin, *J. Am. Chem. Soc.*, 2007, **129**, 12828.
2 M. D. Goodman, J. Xu, J. Wang and Z. Q. Lin, *Chem. Mater.*, 2009, **21**, 934.
3 L. M. Chen, Z. R. Hong, G. Li and Y. Yang, *Adv. Mater.*, 2009, **21**, 1434.
4 B. H. Hamadani, S. Y. Jung, P. M. Haney, L. J. Richter and N. B. Zhitenev, *Nano Lett.*, 2010, **10**, 1611.
5 L. Zhao, X. Pang, R. Adhikary, J. Petrich and Z. Lin, *Angew. Chem., Int. Ed.*, 2011, **50**, 3958.
6 L. Zhao, X. Pang, R. Adhikary, J. Petrich, M. Jeffries-EL and Z. Lin, *Adv. Mater.*, 2011, (in press)..
7 W. L. Ma, C. Y. Yang, X. Gong, K. Lee and A. J. Heeger, *Adv. Funct. Mater.*, 2005, **15**, 1617.
8 V. D. Mihailetchi, H. X. Xie, B. de Boer, L. J. A. Koster and P. W. M. Blom, *Adv. Funct. Mater.*, 2006, **16**, 699.
9 S. Miller, G. Fanchini, Y. Y. Lin, C. Li, C. W. Chen, W. F. Su and M. Chhowalla, *J. Mater. Chem.*, 2008, **18**, 306.
10 H. W. Tang, G. H. Lu, L. G. Li, J. Li, Y. Z. Wang and X. N. Yang, *J. Mater. Chem.*, 2010, **20**, 683.
11 J. Peet, M. L. Senatore, A. J. Heeger and G. C. Bazan, *Adv. Mater.*, 2009, **21**, 1521.
12 Y. Yao, J. H. Hou, Z. Xu, G. Li and Y. Yang, *Adv. Funct. Mater.*, 2008, **18**, 1783.
13 C. Piliego, T. W. Holcombe, J. D. Douglas, C. H. Woo, P. M. Beaujuge and J. M. J. Frechet, *J. Am. Chem. Soc.*, 2010, **132**, 7595.
14 M. He, W. Han, J. Ge, Y. Yang, F. Qiu and Q. Lin, *Energy Environ. Sci.*, 2011, DOI: 10.1039/c1ee01509e.
15 M. He, L. Zhao, J. Wang, W. Han, Y. L. Yang, F. Qiu and Z. Q. Lin, *ACS Nano*, 2010, **4**, 3241.
16 S. S. van Bavel, M. Barenklau, G. de With, H. Hoppe and J. Loos, *Adv. Funct. Mater.*, 2010, **20**, 1458.
17 E. Verploegen, R. Mondal, C. J. Bettinger, S. Sok, M. F. Toney and Z. A. Bao, *Adv. Funct. Mater.*, 2010, **20**, 3519.
18 J. Ge, M. He, F. Qiu and Y. L. Yang, *Macromolecules*, 2010, **43**, 6422.
19 M. He, J. Ge, M. Fang, F. Qiu and Y. L. Yang, *Polymer*, 2010, **51**, 2236.
20 T. Erb, U. Zhokhavets, G. Gobsch, S. Raleva, B. Stuhn, P. Schilinsky, C. Waldauf and C. J. Brabec, *Adv. Funct. Mater.*, 2005, **15**, 1193.
21 Y. Kim, S. Cook, S. M. Tuladhar, S. A. Choulis, J. Nelson, J. R. Durrant, D. D. C. Bradley, M. Giles, I. Mcculloch, C. S. Ha and M. Ree, *Nat. Mater.*, 2006, **5**, 197.
22 L. D. Nielsen, *IEEE Trans. Electron. Dev.*, 1982, **29**, 821.
23 A. G. Aberle, S. R. Wenham and M. A. Green, *Conf. Rec. IEEE Photovoltaic Spec. Conf., 23rd*, 1993, 133.
24 C. Waldauff, P. Schilinsky, J. Hauch and C. J. Brabec, *Thin Solid Films*, 2004, **451–452**, 503.
25 C. W. Chu, H. C. Yang, W. J. Hou, J. S. Huang, G. Li and Y. Yang, *Appl. Phys. Lett.*, 2008, **92**, 103306.
26 C. Waldauf, M. C. Scharber, P. Schilinsky, J. A. Hauch and C. J. Brabec, *J. Appl. Phys.*, 2006, **99**, 104503.
27 P. Schilinsky, C. Waldauf, J. Hauch and C. J. Brabec, *J. Appl. Phys.*, 2004, **95**, 2816.
28 A. Kumar, R. Devine, C. Mayberry, G. Li and Y. Yang, *Adv. Funct. Mater.*, 2010, **20**, 2729.
29 V. Shrotriya, Y. Yao, G. Li and Y. Yang, *Appl. Phys. Lett.*, 2006, **89**, 063505.
30 M. Campoy-Quiles, T. Ferenczi, T. Agostinelli, P. G. Etchegoin, Y. Kim, T. D. Anthopoulos, P. N. Stavrinou, D. D. C. Bradley and J. Nelson, *Nat. Mater.*, 2008, **7**, 158.
31 G. Li, V. Shrotriya, J. S. Huang, Y. Yao, T. Moriarty, K. Emery and Y. Yang, *Nat. Mater.*, 2005, **4**, 864.